High-Fidelity and High-Performance Computational Simulations for Rapid Design Optimization of Sulfur Thermal Energy Storage

Cooperative Research and Development Final Report

CRADA Number: CRD-21-18129

NREL Technical Contact: Zhiwen Ma

NREL is a national laboratory of the U.S. Department of Energy
Office of Energy Efficiency & Renewable Energy
Operated by the Alliance for Sustainable Energy, LLC

This report is available at no cost from the National Renewable Energy Laboratory (NREL) at www.nrel.gov/publications.

Contract No. DE-AC36-08GO28308

Technical Report
NREL/TP-5700-89815
June 2024

High-Fidelity and High-Performance Computational Simulations for Rapid Design Optimization of Sulfur Thermal Energy Storage

Cooperative Research and Development Final Report

CRADA Number: CRD-21-18129

NREL Technical Contact: Zhiwen Ma

Suggested Citation
Ma, Zhiwen. 2024. *High-Fidelity and High-Performance Computational Simulations for Rapid Design Optimization of Sulfur Thermal Energy Storage: Cooperative Research and Development Final Report, CRADA Number CRD-21-18129.* Golden, CO: National Renewable Energy Laboratory. NREL/TP-5700-89815. https://www.nrel.gov/docs/fy24osti/89815.pdf.

NREL is a national laboratory of the U.S. Department of Energy
Office of Energy Efficiency & Renewable Energy
Operated by the Alliance for Sustainable Energy, LLC

This report is available at no cost from the National Renewable Energy Laboratory (NREL) at www.nrel.gov/publications.

Contract No. DE-AC36-08GO28308

Technical Report
NREL/TP-5700-89815
June 2024

National Renewable Energy Laboratory
15013 Denver West Parkway
Golden, CO 80401
303-275-3000 • www.nrel.gov

NOTICE

This work was authored by the National Renewable Energy Laboratory, operated by Alliance for Sustainable Energy, LLC, for the U.S. Department of Energy (DOE) under Contract No. DE-AC36-08GO28308. Funding provided by U.S. Department of Energy Office of Energy Efficiency and Renewable Energy Advanced Manufacturing and Materials Technologies Office. The views expressed herein do not necessarily represent the views of the DOE or the U.S. Government.

This report is available at no cost from the National Renewable Energy Laboratory (NREL) at www.nrel.gov/publications.

U.S. Department of Energy (DOE) reports produced after 1991 and a growing number of pre-1991 documents are available free via www.OSTI.gov.

Cover Photos by Dennis Schroeder: (clockwise, left to right) NREL 51934, NREL 45897, NREL 42160, NREL 45891, NREL 48097, NREL 46526.

NREL prints on paper that contains recycled content.

Cooperative Research and Development Final Report

Report Date: May 1, 2024

In accordance with requirements set forth in the terms of the CRADA agreement, this document is the CRADA final report, including a list of subject inventions, to be forwarded to the DOE Office of Scientific and Technical Information as part of the commitment to the public to demonstrate results of federally funded research.

Parties to the Agreement: Element 16 Technologies, Inc.

CRADA Number: CRD-21-18129

CRADA Title: High-Fidelity and High-Performance Computational Simulations for Rapid Design Optimization of Sulfur Thermal Energy Storage

Responsible Technical Contact at Alliance/National Renewable Energy Laboratory (NREL):

Lead PI: Zhiwen Ma, | zhiwen.ma@nrel.gov

Co-PI: Martin, Michael | Michael.Martin@nrel.gov

Coauthor: Martinek, Janna | janna.martinek@nrel.gov

Name and Email Address of POC at Company:

Dr. Karthik Nithyanandam, Email: karthik@element16.com

Sponsoring DOE Program Office(s):

Office of Energy Efficiency and Renewable Energy (EERE), Advanced Manufacturing and Materials Technologies Office

Joint Work Statement Funding Table showing DOE commitment:

Estimated Costs	NREL Shared Resources a/k/a Government In-Kind
Year 1	$300,000.00
TOTALS	$300,000.00

Executive Summary of CRADA Work:

NREL and Element 16 collaborated on sulfur thermal energy storage modeling using NREL's high performance computing (HPC) resources to assist its application in industrial processes. Industrial process heat (IPH) accounts for ~70% of US manufacturing energy use and is primarily produced by fossil fuel combustion. Approximately, 1500 TWht (~60% Terawatt hour thermal) of IPH demand is in the temperature range of 100-300℃. Industrial applications in this temperature range include drying, hydrothermal processing, thermal enhanced oil recovery, food and beverage, bioethanol production, etc. Cost-effective thermal energy storage (TES) that increases the utilization of waste and renewable heat (solar, geothermal, etc.) could provide significant energy savings and reliable heat sources, decrease emissions, and increase US manufacturing competitiveness through reductions in fuel consumption. This HPC4EI project facilitated Element 16's development of low-cost and high-impact molten sulfur TES for dispatchable IPH. The development of a high-fidelity model validated by experimental data and HPC simulations enabled the successful resolution of the complex interplay between fluid dynamics and heat transfer processes during transient operation of sulfur TES, overcoming the numerical challenges posed by the non-linear temperature-dependent physical properties of sulfur. The project helped accelerate Element 16's molten sulfur TES product design and support its broad applications.

CRADA benefit to DOE, Participant, and US Taxpayer:

- Assists laboratory in achieving programmatic scope,
- Adds new capability to the laboratory's core competencies,
- Enhances the laboratory's core competencies,
- Uses the laboratory's core competencies, and/or
- Enhances U.S. competitiveness by utilizing DOE developed intellectual property and/or capabilities.

Summary of Research Results:

NREL team used high performance computing (HPC) to support Element 16's sulfur thermal energy storage design and development. The CRADA tasks, milestones, deliverables are listed below:

Task 1: Model and Material Property Setup in FLUENT for the Element 16 TES

Subtask 1.1: Develop a 2D free convection model incorporating sulfur properties via User Defined Functions (UDF). Incorporate and compare relative performance of turbulence models with various closure equations under 2D temperature conditions designed to produce laminar, transition, and turbulent natural convection. Benchmark the model against the experimental results in the literature. (**Month 3)**

Subtask 1.2: Build the mesh of the three-dimensional sulfur TES prototype geometry and define boundary and operating conditions. Study meshing approach based on mesh quality metrics. (**Month 3)**

Information flow: Design configuration and geometry, boundary and operating conditions from Element 16 to NREL.

Deliverables: Sulfur TES model setup for HPC run at benchtop scale and the prototype meshing.

Task 2: 3D Prototype Model: Verify Mesh Sensitivity and Validate the Model

Subtask 2.1: Complete grid, time step, and turbulence model verification studies for transient stability and grid independence. (**Month 5)**

Subtask 2.2: Validate the 3D model against prototype test data of various operation cases. Verify results of temperature distributions, flow temperature, heat transfer data inside the sulfur TES against measured values. Simulate the sensitivity of results to H_2S concentration. (**Month 6)**

Information flow: Element 16 provides prototype test data to NREL.

Deliverables: NREL model validation and model accuracy from HPC simulations.

Task 3: Performance Study of Element 16 Sulfur TES Designs

Subtask 3.1: Use validated model to study various TES designs and charging/discharging processes defined by Element 16. Establish a base case of numerical accuracy. (**Month 8)**

Subtask 3.2: Define design parameter space for tube sizing, spacing, number of parallel paths, flow rates, etc. and conduct parametric studies. (**Month 9)**

Information flow: Element 16 provides design objective and operation parameters to NREL.

Deliverables: Design and operation analysis of the sulfur TES performance.

Task 4: Performance Mapping and Model Implementation Adapted by Element 16

Subtask 4.1: Develop a surrogate model or machine-learning model that establishes the functional relationship between performance metrics and design variables or operating conditions and test the predictive validity of the model for new conditions. (**Month 11)**

Subtask 4.2: Develop a design tool based on the surrogate model and implement modeling outcomes for adoption by Element 16 to assess technology-to-market benefits. (**Month 12)**

Information flow: NREL delivers the optimization design assessment tool to Element 16.

Deliverables: A validated model design tool that is capable of design tradeoff and scales, and that can be used for robust multidisciplinary design optimization.

Introduction

State-of-the-art TES uses high freezing point (~220 ℃) molten solar salt in two-tank configuration. However, the two-tank solar salt storage concept for the IPH temperature range of 100-300 ℃ is prohibitively expensive. Other TES options such as latent-based phase change materials (PCMs) and sensible-based solid-state thermal storage media (concrete, rocks) have been extensively investigated but suffer from inherent challenges related to high storage cost, poor thermal responsiveness, and/or thermal cyclic stability concerns.

Element 16 technologies invented a new type of TES, which uses molten sulfur in a single-tank configuration to store and dispatch energy from renewables efficiently and very inexpensively. Element 16's thermal energy storage can charge from electricity or heat, and then discharges heat that can be used directly for industrial processes. Molten sulfur TES provides a low-cost solution to store and deliver thermal energy due to its low cost, high thermal and chemical stability, and high heat transfer rates due to natural convection dynamics within molten sulfur. Sulfur is a cheap commodity at $80/ton compared to $1100 - 1300/ton for conventional salts. When using a metric of storage cost per kWh, sulfur costs around 2-3 $/kWh. Sulfur is orders of magnitude cheaper than alternatives in the temperature range of 100-300 ℃ such as solar salt (44 $/kWh), HitecXL (22 $/kWh), and thermal oil (42 $/kWh), making this an economically viable thermal storage concept for industrial heat supply.

Element 16 has been selected for awards from the California Energy Commission and US Department of Energy to develop the molten sulfur TES technology for combined cooling heat and power systems (CCHP), industrial waste heat capture systems, electrical storage, and solar industrial process heat applications. Pertinent to this project, Element 16 successfully completed installation, testing, and third-party measurement and verification of a 350-kWh molten sulfur TES with gas powered 30-kWe microturbine and absorption chiller to demonstrate the operational flexibility of combined cooling heat and power (CCHP) system with TES. Figure 2 shows the prototype that was commissioned at Element 16's facility in Southern California. The data collected from the prototype testing was used for the validation of numerical model developed in this HPC4ei project.

Figure 1. Element16's 350 kWh sulfur TES prototype

Prototype and Product Storage Modeling Approach

Element 16's sulfur TES design configuration involves heat transfer fluid (HTF) pipes located within molten sulfur stored in a tank. The heat transfer physics is a combination of the forced convection dynamics in HTF and natural convection heat transfer dynamics in molten sulfur. The current 350 kWh pilot system designed for integration with combined heat and power has two different heat transfer fluid circuits inside the TES – one for intaking exhaust from the microturbine for charging and the other circuit flows a thermal oil for discharging the TES. Figure 2 (left) shows a CAD illustration of the 350-kWh pilot molten sulfur TES design that holds 5 ton of sulfur against which the computational model developed by NREL will be validated. Element 16 shared a new product design of sulfur thermal energy storage (TES) for integration with solar thermal. In the new sulfur TES design for integration with solar thermal system, thermal oil is the only heat transfer fluid (HTF) that will flow inside the TES. Excess hot HTF will be routed inside the tube circuit within the TES for storing thermal energy in sulfur and during discharge cold HTF will be pumped to retrieve energy from hot sulfur. The hot HTF exiting the TES during discharge will exchange heat with the process fluid in a separate heat exchanger. Figure 2 (right) shows the engineering drawing of 23-ton sulfur TES prototype that is expected to be commissioned in the fourth quarter of 2023 at Element 16's facility in Duarte, CA.

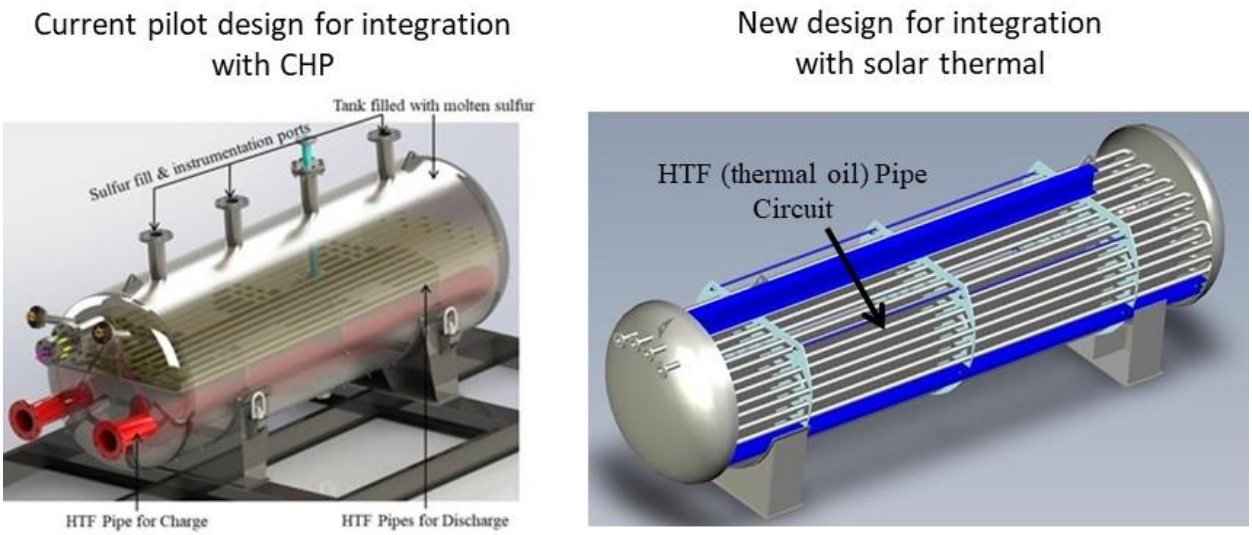

Figure 2. Internal piping layouts of the current pilot design and the product design

Based on the product design, we established design parameters and the 2D computational domain that will be studied in Task 3. The design parameters include HTF tube diameter, transverse and longitudinal spacing between two adjacent tubes — determines the surface area per unit storage capacity (m^2/kWh) for heat exchange —, charge (T_C) and discharge (T_D) temperature. The CFD results coupled with machine learning algorithm will be used to derive Ragone relations that characteries sulfur TES performance for different design and operation parameters. Specifically, CFD results will inform the sulfur side heat transfer coefficient and heat rates expressed in (kW/kWh) as a function of system state of charge. Element 16 is developing an in-house numerical model that will use the heat transfer curves for system performance characterization.

Predicting the transient heat transfer rate in sulfur is critical for design and optimization of these systems in multiple ways. The HTF pipe surface area requirement is determined by this rate. More importantly, the transient exit HTF temperature during discharge, a key indicator of quality of the energy recovered from the storage system (second-law efficiency) depends on the HTF tube arrangement and HTF flow path in the tank such that the exergy destruction due to thermal-buoyancy-induced mixing is minimized. Element 16 performed initial design simulations using a representative two-dimensional unit cell, constant surface temperature boundary condition at the HTF pipe and constant sulfur thermophysical properties. This is in keeping with Element 16's current computational capabilities of an 18-processor workstation.

However, the TES product performance is closely tied to the three-dimensional spatial and temporal evolution of both sulfur and HTF temperatures. *The thermal-buoyancy-induced mixing and corresponding heat transfer rates are a strong function of sulfur thermophysical properties, which can exhibit large and rapid variation with respect to local temperature conditions or concentration of impurities*. Inclusion of these thermophysical property variations requires customization of the computational fluid dynamics (CFD) code and can have implications on simulation stability and convergence properties. Hence, a three-dimensional transient thermo-fluid characterization including all relevant property variability and using high-performance computing (HPC) resources is critical in optimizing the product design for both cyclic performance (exergetic efficiency, round-trip efficiency) and lifetime cost.

Results and Explanation

Task 1. 2D/3D modeling of prototype sulfur TES and model validation against test results.

NREL obtained prototype testing data of a 350-kWht sulfur TES system for 3D validation from Element 16. NREL simulated 3D model prototype with charge and discharge pipes as shown in Figure 2. The CFD simulation was conducted using ANSYS Fluent and with temperature dependent sulfur properties with 35 ppm H_2S impurities. 3D mesh used for the prototype model shown in Figure 3 had 800K hexahedral cells with the inflation layer around charge and discharge pipes to capture near wall heat transfer and temperature gradient accurately.
In addition to employing UDF's for sulfur properties and impurities, another UDF was also implemented to establish boundary condition for the charge and discharge pipes. The data obtained from Element16 provided inlet and outlet temperature for the HTF fluid inside charge and discharge pipes. UDF was solved once per time step using an internal sub-timestep for stability of explicit finite difference methods to calculate fluid temperature along the axial dimension and was also used to set the wall boundary condition for the next time step. Convective boundary condition at tube walls is updated at every time step using computed HTF temperature and HTF heat transfer coefficient from Gnielinski correlation evaluated at local conditions.

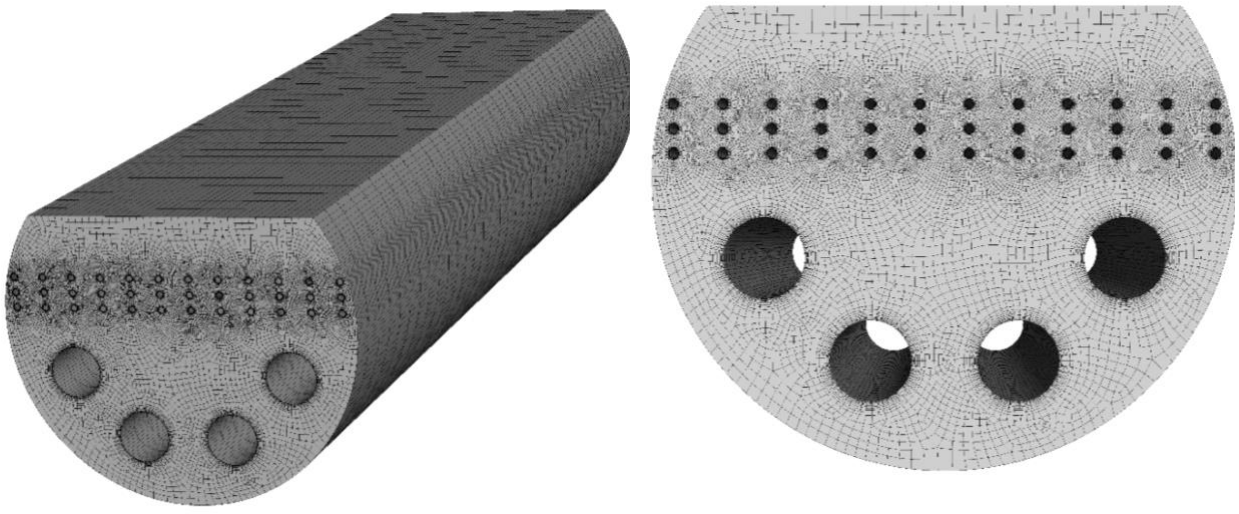

(a) isometric *(b)* front view

Figure 3. Structured mesh for prototype: charge (top) and discharge pipes (bottom) have inflation layers to capture near wall temperature gradients.

Figure 4 shows the temperature gradient across charge pipes based on UDF. Air at higher temperature enters charge pipes, navigates through four passes, and exits at lower temperature by charging sulfur inside domain to higher temperature. Top view of the charge pipes in Figure 4 (a) shows traces of high temperature location across the length, elucidating convection of sulfur and location of plume detachment from charge pipe. The bottom view in Figure 4 (b) shows the lower temperature side of charge pipes. Evident temperature difference in Figure 4 (a) and (b) for charge pipes facilitates natural convection through radial temperature gradient.

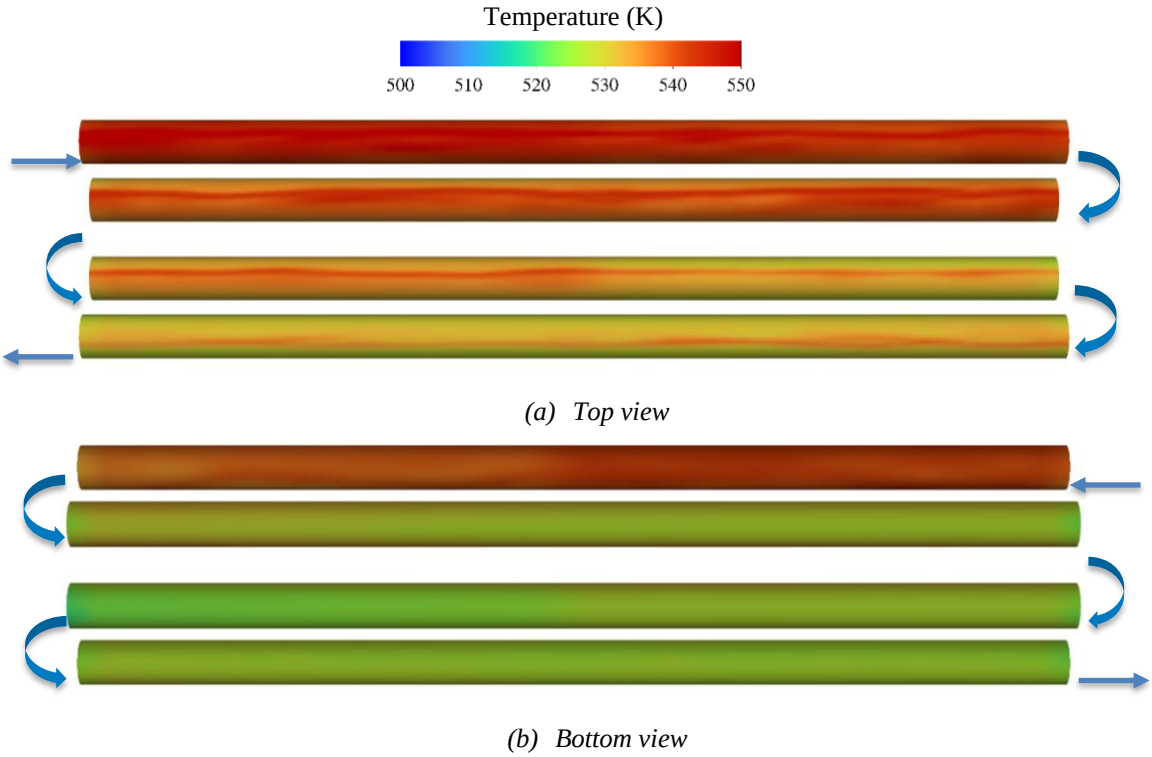

(a) Top view

(b) Bottom view

Figure 4. Temperature along length of charge pipes based on UDF at 11.11 hr.

Element16 collected sulfur temperature at different radial and axial positions for its pilot system experiment. The data shown in Figure 5 compares the temperature at 17 different locations obtained from 3D simulations with experiments. The results presented are here at 11.11 hr into the simulation, i.e., for charging. The overall trend of temperature at discrete locations with time can be said to be in good agreement with the experimental data. Three outliers P1, P11 and P12 were found exhibiting different trends than experimental data. Specifically, P1 and P11 were located at Y=-23.3", almost at the bottom of the prototype tank. Point P12 located at Y=-18" was a better fit than P1 and P11. The disagreement was found to be at the low temperature region in 3D simulation (see temperature profiles in Figure 6) spanning across length of tank.

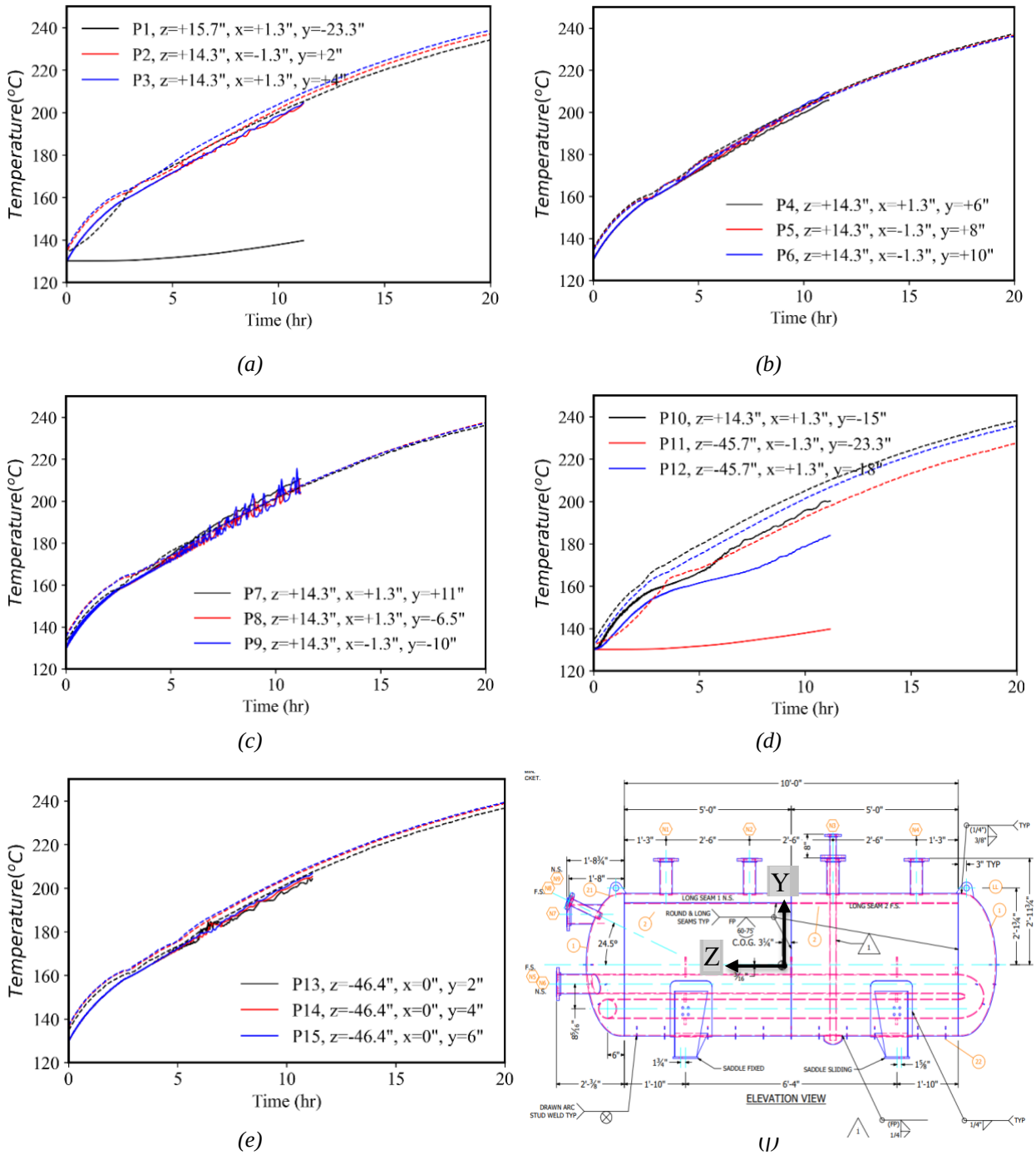

Figure 5. Temperature at different location (a-e) within prototype domain compared with experiment (f). Experiment was conducted on a 350-kWht (kilowatt hour thermal) sulfur TES system of Element16. The pilot system experiment was operated by varying the HTF flow rate and inlet temperature to TES so that the transient molten sulfur temperature data for various operation conditions were recorded at different radial and axial locations. Radial and axial positions reported (a-e) can be visualized based on co-ordinate system shown for the TES system(f).

In experiments conducted by Element16, a heater with a constant 1 kW input was placed at the bottom of the tank to account for heat losses through system. The heater input in the experiment led to higher 'local' temperature at discrete points at the bottom of the tank. Based on excellent agreement at other discrete locations, it can be said that the heat addition at the bottom of the tank neglected in 3D simulations had only local effects and did not affect overall 3D heat transfer conditions. NREL concludes that the developed 3D computational TES model is validated with Element16's experiments for charging conditions.

Task 2. 3D effects in TES prototype:

3D computations for a natural convection problem can be extremely challenging and time consuming. Although NREL has shown that 3D sulfur TES can be modeled using CFD, the two-dimensionality of heat transfer mechanism within the TES can be useful in ML modeling and optimization of system. Contours shown in Figure 6 are at five different locations across its span at z = 1.7, 0.935, 0, -0.935, and -1.7 m. The contours of velocity magnitude exhibit that flow pattern is somewhat similar across tank span with minimal axial flow perturbations. It can be observed through temperature contours that plume from cylinders rises and forms a circulation region. Low viscosity sulfur from bottom of the tank and near cylinder region rises due to temperature gradient to high viscosity region at the top of the tank as shown in Figure 6.
The circulation behavior can be confirmed by velocity contours and streamlines shown in Figure 7. Streamlines across vertical plane in Figure 7(a) elucidate flow from bottom of the tank to top and Figure 7(b) shows flow across charge channels i.e., X direction. It is preliminary because each charge tube is at different temperatures, giving rise to temperature gradient in the X direction i.e., across width of tank. Hence, the flow across width becomes more dominant than the flow across axis or span of tank, minimizing axial flow effects. Volume averaged temperature and viscosity values from 3D simulation were also compared against the surface averaged values in Table 1. Surface averaged values show that a 2D cross section from the prototype tank can give an accurate representation of the bulk average temperature and viscosity in tank, reaffirming that spanwise flow and 3D effects are minimal during charging of sulfur within TES.

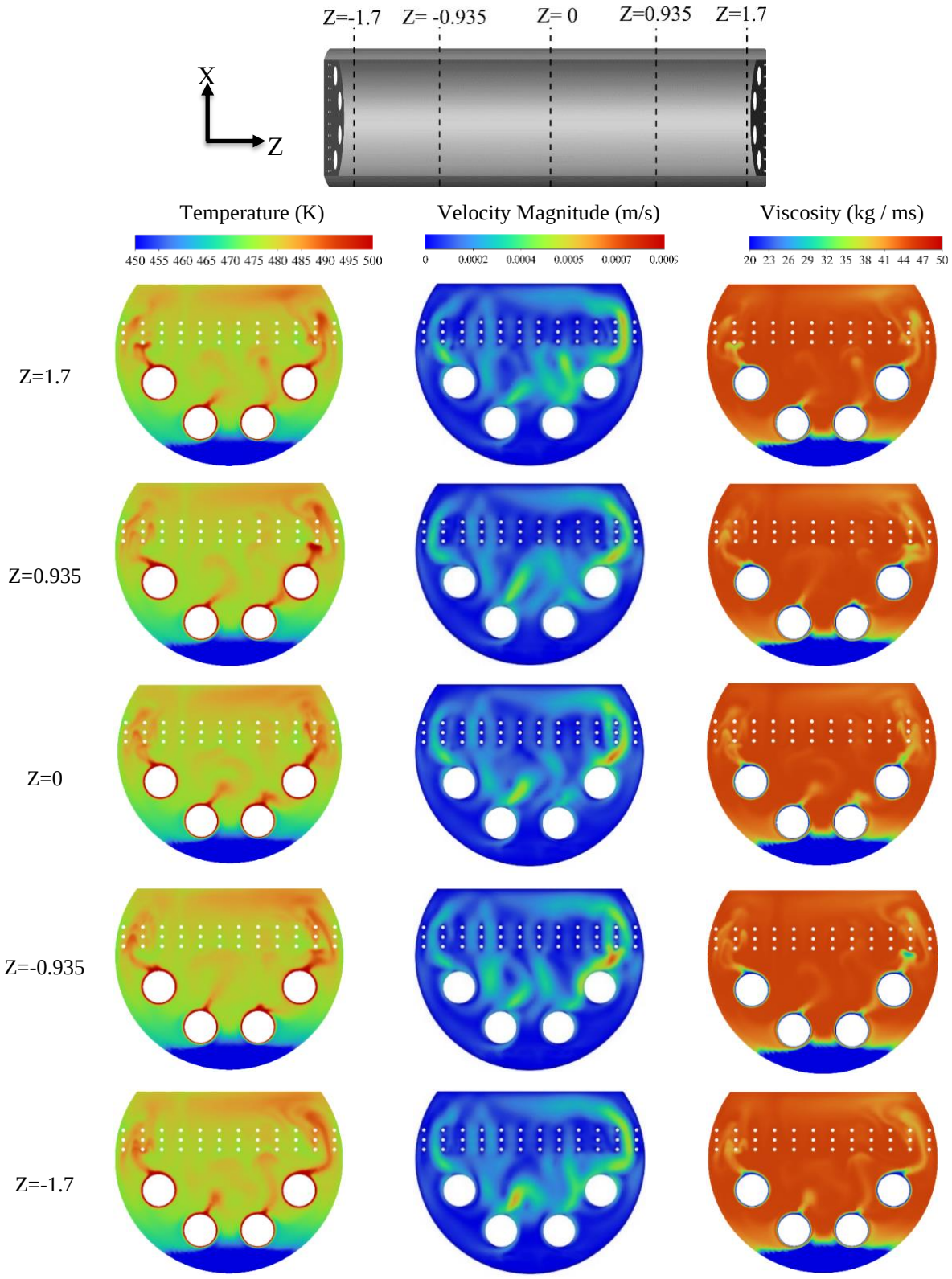

Figure 6. Contours of temperature, viscocity and velocity magnitude at prototype tank span location of 1.7, 0.935, 0, -0.935, and -1.7 m at 11.11 hr.

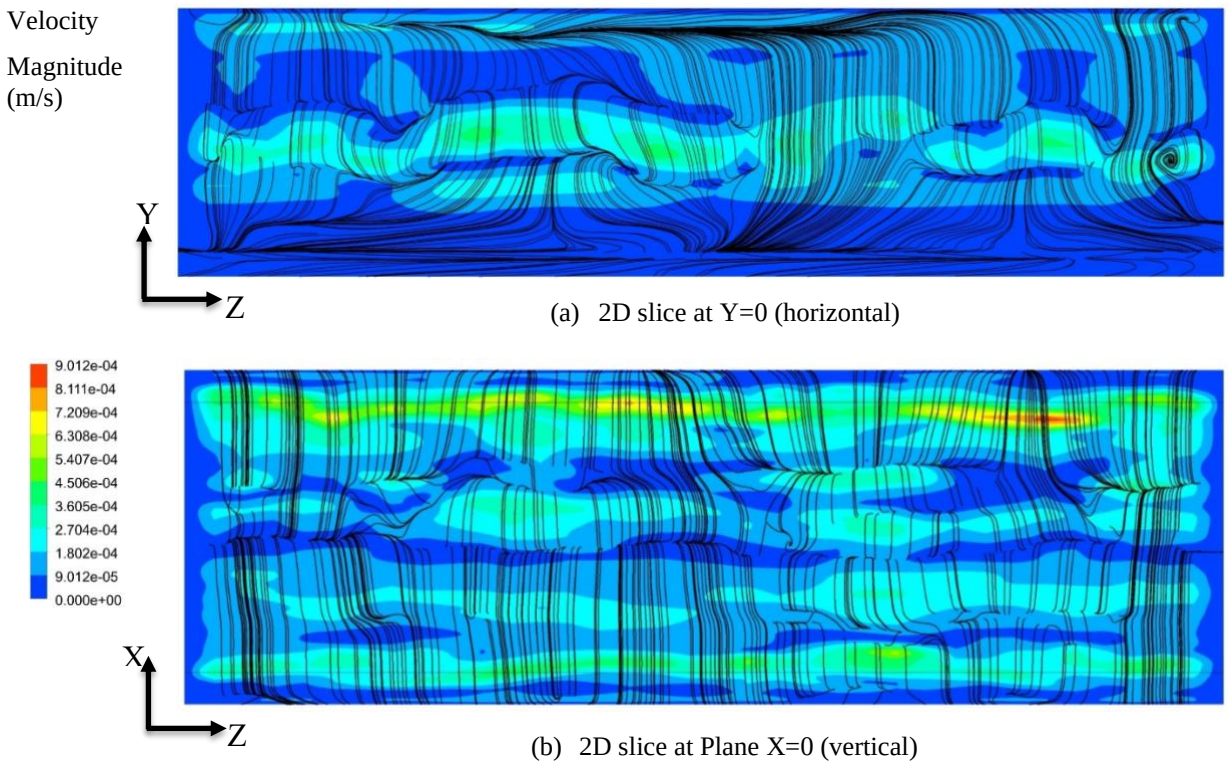

Figure 7. Streamlines imposed on velocity contours across (a) Y=0 and (b) Z=0 plane for prototype, exhibiting flow pattern acorss spanwise direction at 11.11 hr.

Table 1. Comparison of surface averaged properties across different span length of the tank.

Location	$\bar{T}$ (K)	$\bar{\mu}$ (kg/ m s)
Total (Volume averaged)	475.65	40.04
z= -0.935 (Surface averaged)	475.78	40
z= -1.7 (Surface averaged)	475.77	39.97
z= 0 (Surface averaged)	475.64	40.01
z= +0.935 (Surface averaged)	475.54	40.10
z= +1.7 (Surface averaged)	475.56	40.07

Task 3. Performance Study of Element 16 Sulfur TES Designs

Based on validated 2D/3D CFD models developed in Task 2, we studied the effect of various TES design parameters on charging/discharging processes as defined by Element 16. With many design parameters including tube sizing, spacing, number of parallel paths, flow rates, etc. we conducted parametric studies on sensitive factors with rapid empirical modeling approach, and established a base case of numerical accuracy. The design tool based on the surrogate model was also extended to Machine-Learning (ML) in Task 4 for design and operation analysis of the sulfur TES performance. The modeling outcomes were implemented for Element 16 adoption to assess technology-to-market benefits.

This analysis shows that literature correlations are of limited utility in modeling liquid sulfur natural convection, as nondimensionalization of heat transfer physics cannot be adequately performed in the presence of complex property variations. While dimensionless models are the most computationally inexpensive way of correlating results from CFD simulations to scalable industrial systems, the data shows that standard definitions of the Nusselt and Rayleigh numbers cannot produce accurate representations of heat transfer for an elementary steady-state case, let alone the transient sulfur TES process. We conclude that achieving rapid optimization of molten sulfur TES, or of any system using a working fluid with highly non-linear properties, will require a more detailed approach for predicting heat transfer, whether that be utilizing alternate methods to construct case-specific dimensionless correlations or abandoning the use of dimensionless correlations in the design process altogether.

The model used in this work is a system of steady-state free convection in concentric cylinders, as shown in Figure 8. The annular fluid is sulfur with 35 ppm H_2S impurities, operating in the temperature range of 400-600 K. The fluid region is bounded by an inner cylinder of radius r_i = 0.02 m and an outer cylinder of radius r_o = 0.1 m. The inner and outer cylinder walls are at constant temperatures T_i and T_o, with cellular flow generated by the temperature gradient across the annular space. The geometry resembles that of a TES system with an uninsulated outer wall maintained at the initial temperature of the fluid, which is not an existing or likely TES configuration.

The computational model in this study was first verified by simulating the system with air in the annular space, a fluid whose thermophysical properties are standard and well-established. Studies of free convection heat transfer through horizontal cylinders with air or water as the fluid medium often list $\pm$10% variation as the criteria for acceptable accuracy when comparing empirical literature correlations to experimental data or numerical solutions.

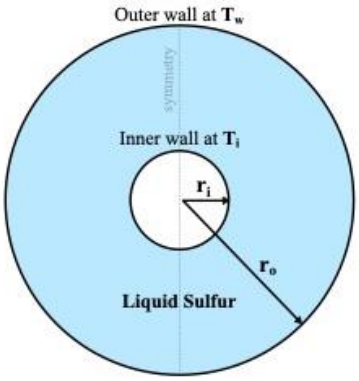

Figure 8. CFD model of the 2D concentric cylinder free convection system with dimensions and boundary conditions.

Figure 9 shows comparisons of heat transfer data from CFD simulations to both the Raithby and Hollands – R&H (1975) and Kuehn and Goldstein – K&G (1976b) correlations for air in horizontal concentric cylinders when T_o = 400 K and T_o = 500 K.

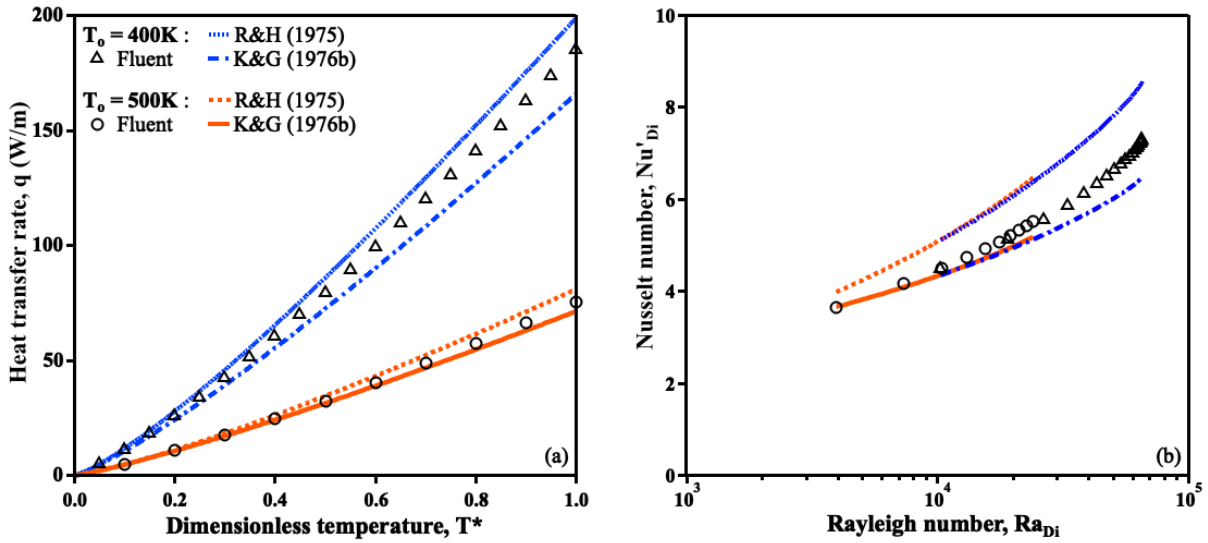

Figure 9. Comparison of heat transfer results from literature correlations to those from CFD simulations for air in concentric cylinders with outer wall temperatures of 400 K and 500 K. (a) q vs. T* where T* = (Ti-To)/(600-To), (b) Nu'Di vs log10(RaDi).

Following CFD model verification, simulations were conducted for the concentric cylinder geometry with 35 ppm H_2S sulfur replacing air as the annular fluid. Calculations (1)-(11) were performed for outer wall temperatures varying between 400 K and 580 K. Inner wall temperatures were assigned values greater than T_o, up to 600 K. Table 1 provides a full list of the 87 cases that were simulated. The most extreme variations of liquid sulfur fluid properties occur in the lower temperature regime, below a temperature of ~ 450 K. Comparison of R&H (1975) and K&G (1976b) predictions to results from CFD simulations for outer wall temperatures >= 460K are shown in Figure 10.

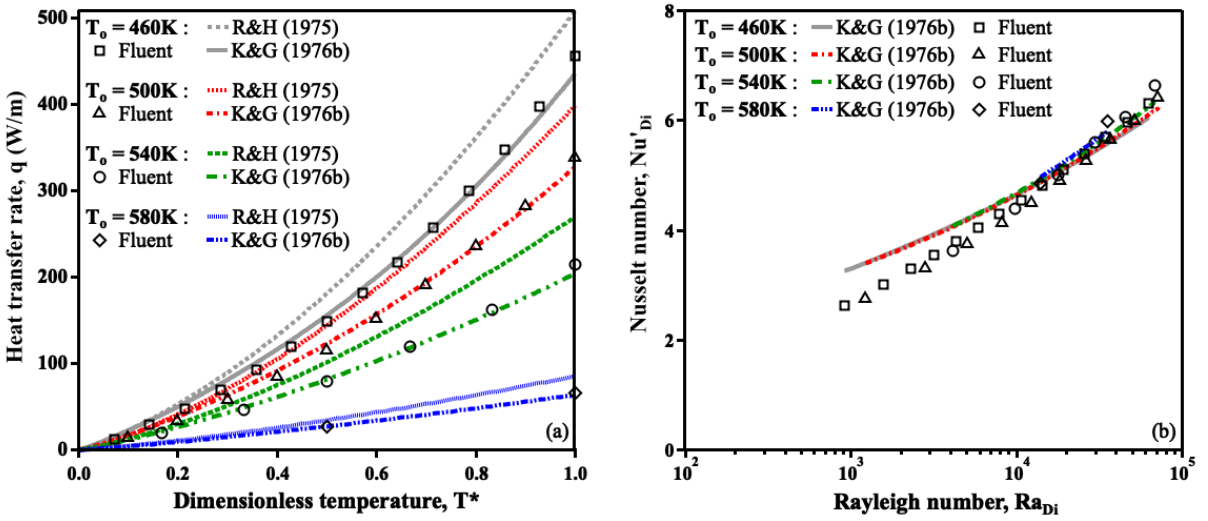

Figure 10. Comparison of heat transfer results from literature correlations to those from CFD simulations for sulfur in concentric cylinders with outer wall temperatures >= 460 K. (a) q vs. T* where T* = (Ti-To)/(600-To), (b) Nu'Di vs log10(RaDi).

The results demonstrate the extent to which extreme fluid property variations impact the ability of correlations to make accurate predictions of heat transfer. Figure 11a illustrates that when the outer wall temperature is dropped down to 440 K, the level of accuracy in heat transfer rates predicted by the correlations resembles that of the higher temperature regime. The K&G (1976b) model underestimated CFD results by a maximum of 21%, with over a third of the deviations from data points remaining within 15%. Coincidentally, the R&H (1975) model produced extremely accurate predictions for this outer wall temperature, with a maximum variation of ±5%. Regardless, the lack of consistency in the R&H (1975) correlation across temperatures both above and below 440 K provides strong evidence of its invalidity in this application. While the most obvious fluctuations in the fluid properties of 35 ppm H_2S sulfur take place during a temperature increase from 430 K to 450 K, the results show that self-similar predictions of heat transfer can still be made by the literature correlations at temperatures as low as 440 K. Figure 11b,c suggests that it is not until the inner to outer wall temperature gradient encompasses the sulfur polymerization transition temperature (~ 430 K) that both correlations become completely invalid.

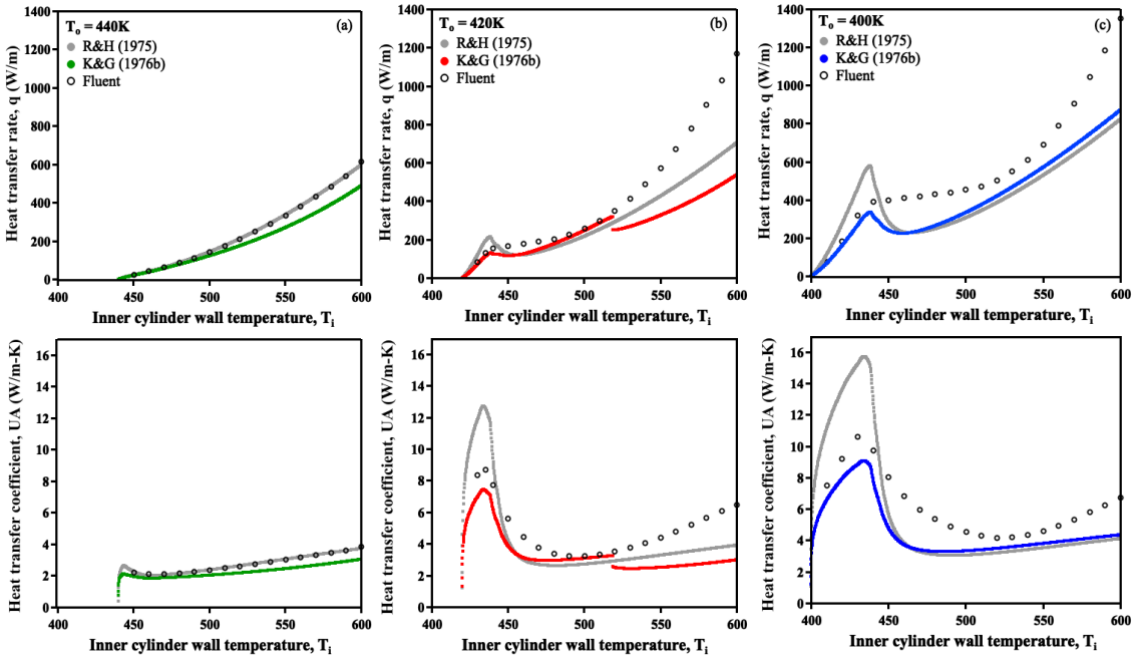

Figure 11. Comparison of heat transfer rates and heat transfer coefficients from empirical correlations to those from CFD simulations for sulfur in concentric cylinders with outer wall temperatures at (a) To = 440 K, (b) To = 420 K, and (c) To = 400 K.

Empirical correlations for free convection in concentric cylinders operate on the assumption that if $T_i > T_o$, cellular flow will follow a pattern of symmetric ascension along the inner cylinder and descension along the outer cylinder [46]. The results in

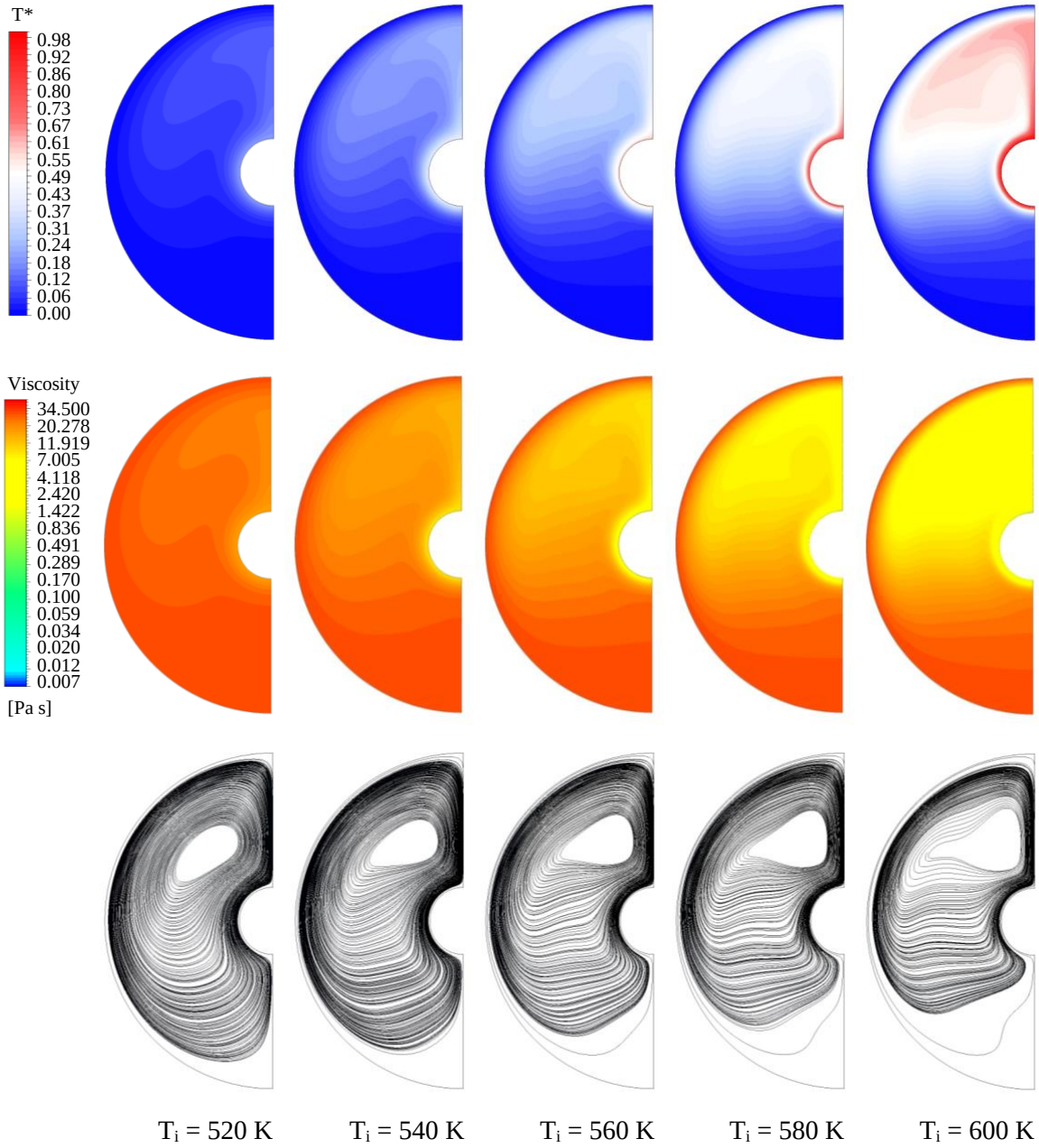

Figure 12 suggest that buoyancy-driven flow patterns of sulfur at temperatures between 500 K and 600 K exhibit this behavior and maintain a steady semicircular current regardless of the size of the temperature gradient across the fluid region. An increase in temperature difference between the cylinder walls does generate more localized flow activity that is concentrated in the top half of the annular space, causing an increase in temperature nonuniformity throughout the sulfur medium. Still, the general flow path remains consistent and matches expectations of the

correlation, thus substantiating the self-similarity of K&G (1976b) predictions across higher temperatures.

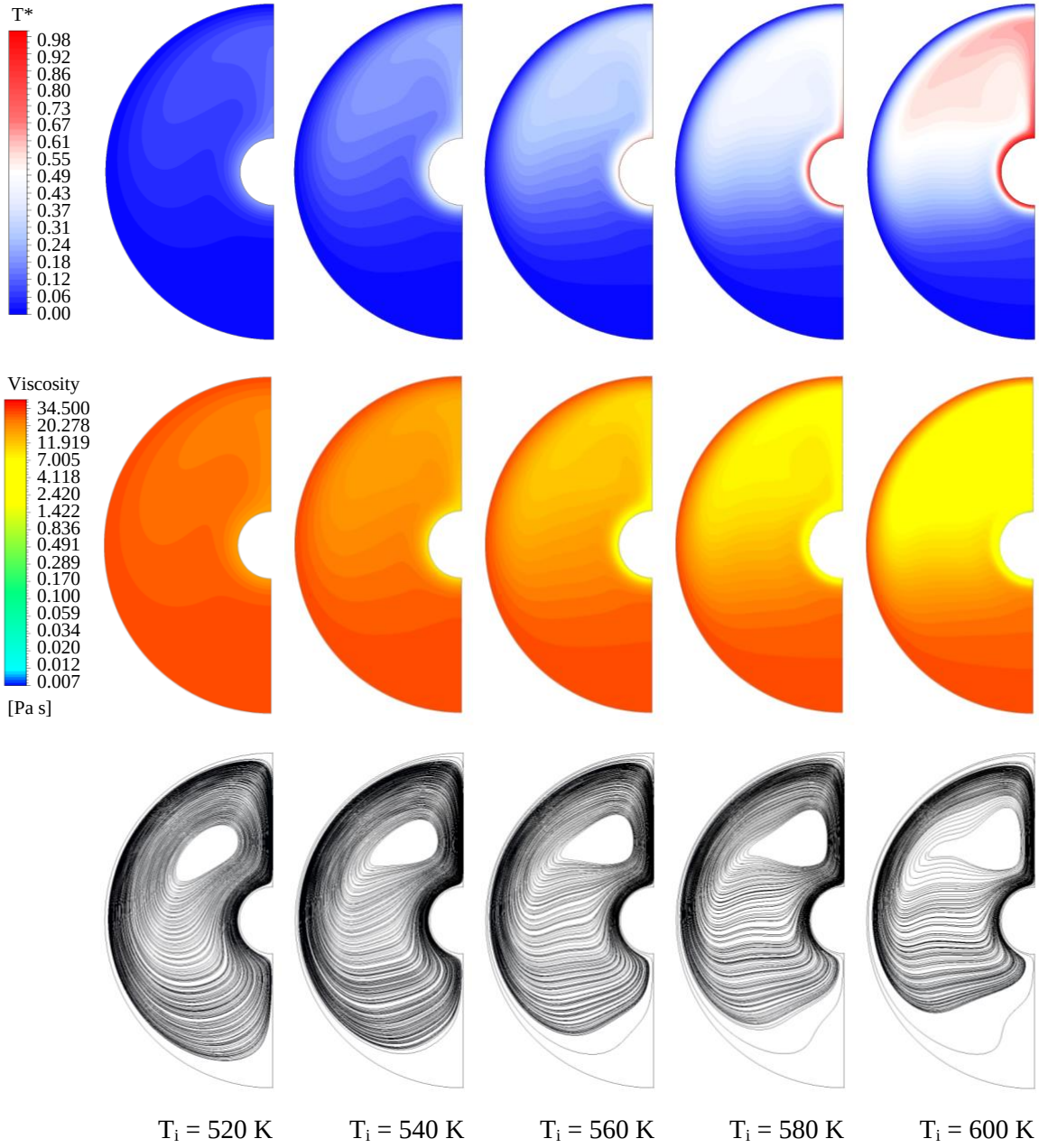

Figure 12. Dimensionless temperature contours, log-scale viscosity contours, and velocity streamlines for sulfur in concentric cylinders when the outer wall temperature is 500 K. Cases depicted are for inner wall temperatures ranging from 520-600 K.

Task 4. Performance Mapping and Model Implementation

This section introduces machine learning (ML) development for validated model design tool that is capable of design tradeoff and scales. This work developed a surrogate model or ML model that establishes the functional relationship between performance metrics and design variables or operating conditions. Figure 13 shows the ML computational workflow. Various ML algorithms were used to test the predictive validity of the model for new conditions.

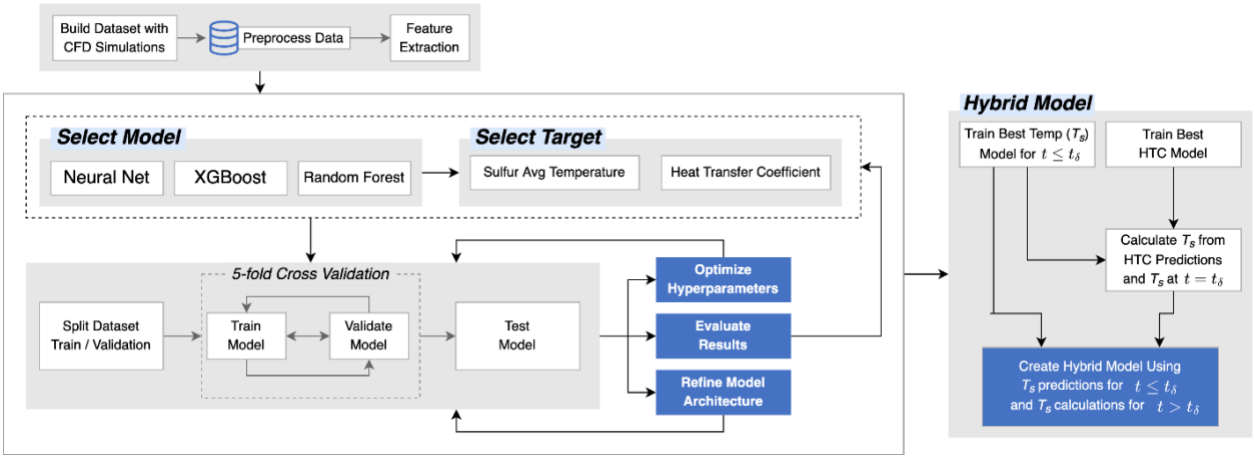

Figure 13: The ML-based computational workflow.

The hyperparameters for the three models (XGBoost, Random forest, and NN) were optimized with Optuna [1]. For the XGBoost and Random Forest models, the hyperparameters were optimized to predict HTC. For the NN model, the hyperparameters were optimized to predict temperature. A visualization of the optimization process is displayed in the figures below.

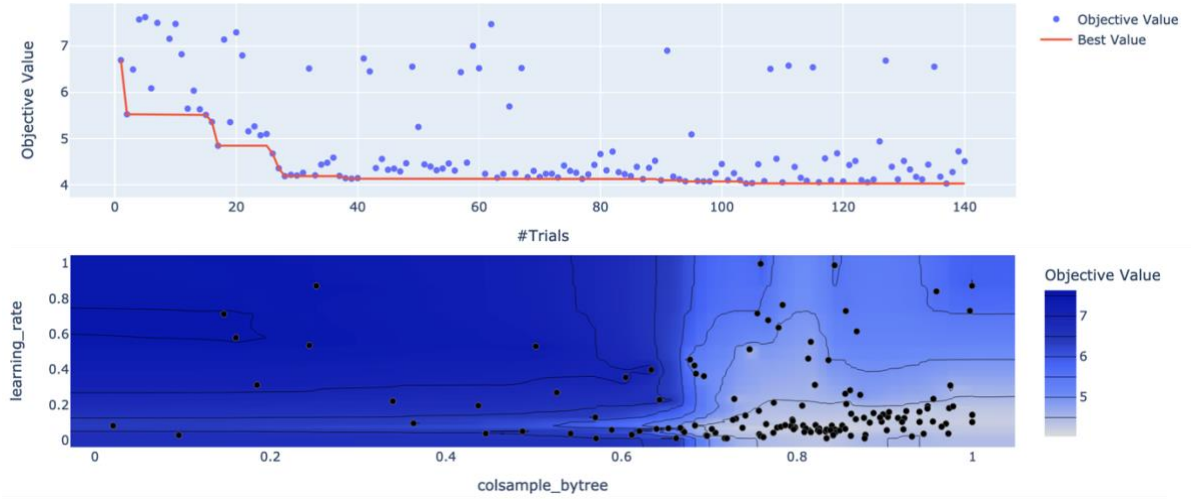

Figure 14. Visualizations of the Optuna hyperparameter optimization process. The top chart shows the study progress, with the objective value (RMSE) being minimized. The bottom chart shows a contour plot visualization of the best values for two hyperparameters. The lighter area is where the objective value is minimized. Notice the cluster of trial results within the lighter area, which is expected.

The models were trained and validated using a five-fold cross validation process and early stopping was implemented for the XGBoost and NN models. The results of this training with optimized hyperparameters are summarized in the table below:

Table 2. Predicting Ts and h with Optimal Hyperparameters

	R2	RMSE
XGBoost (h)	.999	2.65 W/m2K
RandomForest (h)	.998	3.43 W/m2K
NN (Ts)	.998	2.08 K

Using the predictions for heat transfer coefficient from the XGBoost and Random Forest models, the average sulfur temperature at each timestep can be calculated with the following formula:

$$T_{s,i+1} = T_{s,i} + \frac{h_i A_s (T_w - T_{s,i})}{mc_p} \Delta t \qquad (1)$$

i - Current timestep, A_s - Heat transfer surface area, m - sulfur mass, c_p - specific heat, Δt – timestep size

Similarly, using the predictions for sulfur average temperature from the NN model, the heat transfer coefficient at each timestep can be calculated with the following formula:

$$h_{i+1} = \frac{mc_p}{A_s (T_w - T_{s,i})} \frac{T_{s,i+1} - T_{s,i-1}}{2\Delta t} \qquad (2)$$

A sample of the results of calculating one property from another is displayed in Figure 15 and Figure 16.

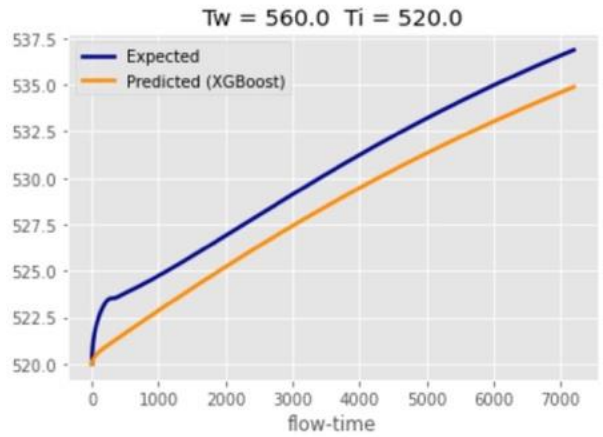

Figure 15. Calculating T_s from h

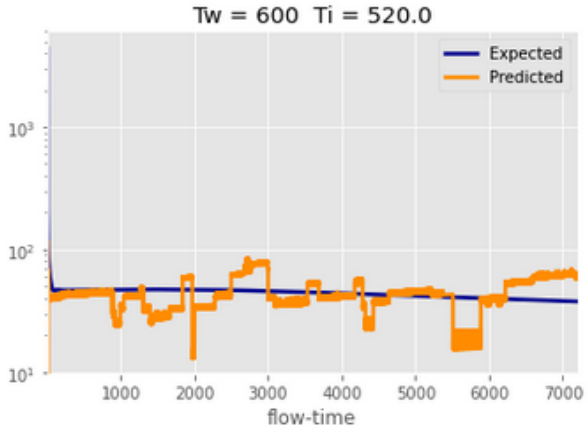

Figure 16. Calculating h from Ts

The calculation of HTC from temperature suffers from errors due to the variance in the time derivative of temperature. This variance is caused by erroneous fluctuations in the NN model predictions of temperature. There is error in the calculation of T_s from h during the initial phase of heat transfer. The CFD simulation data shows a rapid rise in T_s during the first few hundred seconds. This rapid rise is not seen in the calculation of T_s from HTC predictions. This error occurs even when using the value of HTC output from the CFD to calculate T_s. The cause of this error is a discrepancy between the way T_s and h are calculated in the CFD simulations, which, while worthy of mentioning here, is outside the scope of this paper.

To rectify this error, a hybrid model was built using both predictions of T_s and calculations of T_s from HTC predictions. The hybrid model consists of an NN model trained to predict T_s for $t \leq 360$ and calculations of T_s from the XGBoost model h predictions for $t \geq 360$. The value for T_s at t=360 is provided as the initial point for calculating T_s from HTC predictions. The cutoff time of 360 seconds was chosen to align with the length of the truncated datasets mentioned earlier. The results of training and testing this hybrid model are displayed in the table and figures below.

Table 3. Hybrid Model Predictions of Temperature

R2	RMSE	Average % Error
.9998	0.613 K	< 0.2%

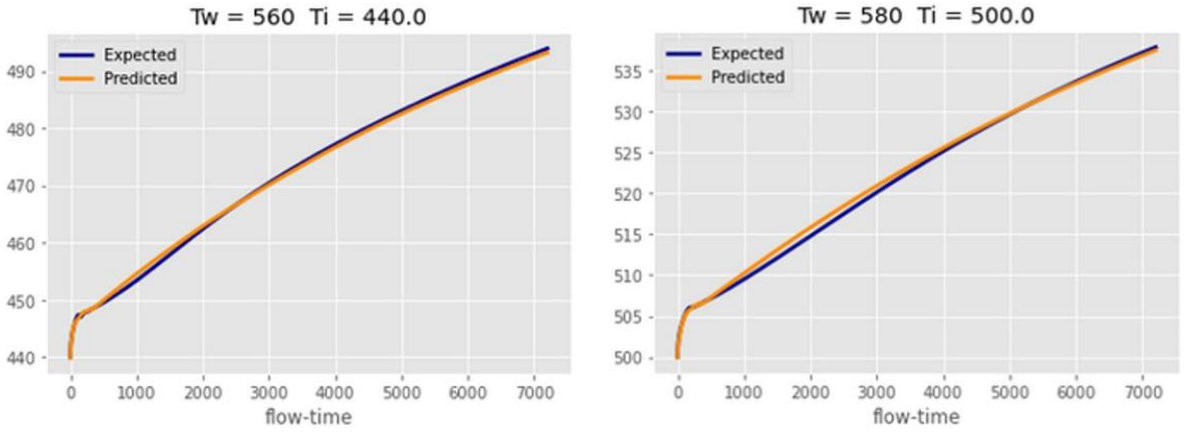

Figure 17. A sample of the results of the hybrid model predictions of Ts. Note the error prevalent in the results shown in Figures 15 and 16 has been eliminated with this model.

The hybrid model demonstrates significant improvement in predicting T_s. Using the NN model to predict T_s for the first 360 seconds successfully eliminated the error apparent in Figures 15 and 16. This hybrid model for predicting T_s, taken along with the XGBoost model for predicting h amounts to a set of accurate models capable of performing as surrogates for the CFD simulations. These models can be further developed by generating training data for more complex systems as well as for discharging scenarios and refining the models to perform well with the new dataset.

Results of the per-scenario model evaluation are displayed in Figure 18. From these results, it is clear the XGBoost and Neural Network models performance declines at the periphery of the training dataset. This is not the case for the performance of the hybrid model, which presents no clear pattern.

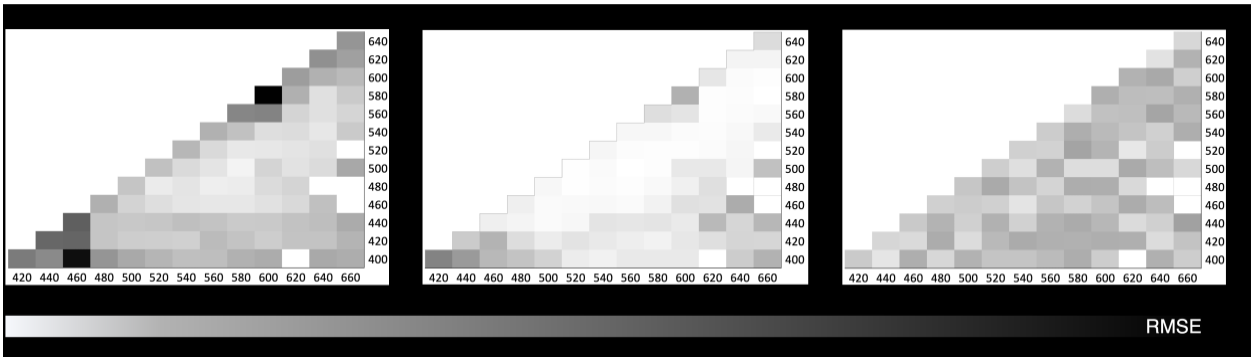

Figure 18. The results of the per-scenario evaluation of the final models. This evaluation process helps identify regions of high or low accuracy, such as the two outlier scenarios (in black) observed at (460,400) and (600,580) for the XGBoost model for h.

Final Task. CRADA Final Report

This report serves to meet the requirement for the CRADA Final Report with preparation and submission in accordance with the agreement's Article X.

Subject Inventions Listing:

None.

ROI #:

None.